



Improved Distribution and Uniformity of α -Al(Mn,Cr)Si Dispersoids in Al-Mg-Si-Cu-Mn (6xxx) Alloys by Two-Step Homogenization

ZHEN LI, JIAN QIN, HAITAO ZHANG, XIAOGUO WANG, BO ZHANG, and HIROMI NAGAUMI

The recrystallization behaviors of deformed 6xxx aluminum alloys can be effectively controlled with α -Al(Mn,Cr)Si dispersoids by pinning or slowing the movement of dislocations. However, abnormal grain growth still often occurs due to the nonuniform distribution of α -Al(Mn,Cr)Si dispersoids. In the present study, the uniformity of dispersoids was significantly improved by applying two-step homogenization heat treatments. The effect of different homogenization conditions on the distribution of the α -Al(Mn,Cr)Si dispersoid was evaluated. By applying traditional one-step homogenization at 550 °C for 10 hours, the dispersoids exhibited sparse and nonuniform precipitation at the center of grains or dendritic arms. These areas with a nonuniform distribution of dispersoids were regarded as coarse dispersoid zones (CDZs). Relative to one-step homogenization, two-step homogenization led to a considerable reduction in the percentage of CDZ area from approximately 7 pct to less than 2.5 pct. This result was due to the diffusion of solute elements and the precipitation of metastable Mg_2Si and Q phases because of isothermal holding during the first step. Metastable Mg_2Si and Q phases could act as nucleation sites to promote the precipitation of α -Al(Mn,Cr)Si dispersoids. As a result, α -Al(Mn,Cr)Si dispersoids exhibited uniform precipitation, and the formation of CDZs was avoided. Two-step homogenization also improved the recrystallization resistance of the alloy because of the decrease in the percentage of CDZ area.

<https://doi.org/10.1007/s11661-021-06243-3>

© The Minerals, Metals & Materials Society and ASM International 2021

I. INTRODUCTION

OWING to the excellent combination of strength, ductility, processing ability, and corrosion resistance, Al-Mg-Si (6xxx) alloys are widely used commercially in the architectural, electronic, and automobile industries. Thermal deformation (such as extrusion and forging) is often applied to 6xxx aluminum alloys after homogenization. However, peripheral coarse grains and abnormal grain growth often occur during extrusion or forging processes. These issues need to be effectively

solved to avoid poor surface quality and uneven mechanical properties.^[1,2] A uniform microstructure is particularly important for materials applied in automobile components, which require high performance and durability.

The recrystallization of deformed grains can be effectively controlled using α -Al(Mn,Cr)Si dispersoids by pinning or slowing the movement of dislocations and grain boundaries.^[3–5] The precipitation temperature of α -Al(Mn,Cr)Si dispersoids is approximately 340 °C.^[6,7] In addition, α -Al(Mn,Cr)Si dispersoids are thermally stable at elevated temperatures^[6,8,9] and are smaller than 200 nm,^[7] even at homogenization or solution temperatures. Thus, α -Al(Mn,Fe)Si dispersoids can effectively slow the recrystallization of 6xxx aluminum alloys during hot deformation, annealing, or solution treatment.

The chemical composition of alloys also significantly influences the precipitation behaviors of α dispersoids. The addition of Mn can promote the precipitation of α -Al(Mn,Fe)Si dispersoids.^[10] Cu can improve the thermal stability of α -dispersoids.^[11] Dispersoids tend to decrease in size with the addition of Si.^[12] Mg markedly affects the precipitation behaviors of

ZHEN LI, JIAN QIN, and HIROMI NAGAUMI are with the High-Performance Metal Structural Materials Research Institute, Soochow University, Suzhou, 215021 Jiangsu, P.R. China and also with the Shagang School of Iron and Steel, Soochow University, Suzhou, 215021 Jiangsu, P.R. China. Contact e-mails: jian.qin@uqac.ca, zhanghai888jp@suda.edu.cn HAITAO ZHANG is with the Key Lab of Electromagnetic Processing of Materials, Ministry of Education, Northeastern University, Shenyang, 110819 Liaoning, P.R. China. XIAOGUO WANG is with the College of Engineering, Shanxi Agricultural University, Taigu, 030801 Shanxi, P.R. China. BO ZHANG is with the Shandong Weiqiao Pioneering Group Co., Ltd, Zouping, 256200 Shandong, P.R. China.

Manuscript submitted October 22, 2019; accepted March 10, 2021.

Article published online May 26, 2021

α -Al(Mn,Fe)Si dispersoids by influencing the nucleation of these dispersoids. The intermediate phases “u-phase,” β' -Mg₂Si, β'' -Mg₂Si, and Q'-AlMgSiCu have been reported to be nucleation sites for α -dispersoids.^[11,13–15] Owing to the presence of nucleation sites, the amounts of α -dispersoids multiply.

During the industrial production of wrought 6xxx alloy products, α -Al(Mn,Cr)Si dispersoids will precipitate during homogenization,^[16,17] which needs to be performed cautiously to control the nucleation and precipitation of α -dispersoids. Many studies have been conducted on the homogenization of 6xxx alloys. Traditional industrial homogenization treatments of AA6xxx alloys usually heat materials to high temperatures (500 °C to 600 °C) at a constant heating rate, and the microsegregation of solute elements is eliminated^[18] by extending the holding time or increasing the homogenization temperature. Another objective is to dissolve intermetallic particles with a low melting point, such as Mg₂Si and Q intermetallics formed during casting, to increase the strength and ductility of materials.^[18–20] Homogenization can also be used to transform β -Al₅FeSi to the α -Al₁₂(Fe,Mn)₃Si intermetallic phase^[20–23] to enhance the formability of the materials. However, the control of α -dispersoids is often neglected in the traditional industrial homogenization of 6xxx alloys. The effect of homogenization heat treatment on the distribution of dispersoids in 6xxx Al alloys is also rarely reported.

The current study aimed to eliminate the nonuniform distribution of dispersoids by two-step homogenization. The nonuniform distribution areas of the dispersoids were observed by dark-field optical microscopy, scanning electron microscopy (SEM), and transmission electron microscopy (TEM). The percentage of CDZ area was also quantitatively characterized. EBSD was employed to evaluate the effect of α -dispersoid distribution on the hot deformation microstructure. The microsegregation of elements caused by casting was evaluated by EPMA testing. A possible mechanism of dispersoid nucleation and precipitation during two-step homogenization was proposed.

II. EXPERIMENTAL

Ingots with a diameter of 152 mm prepared by direct chill (DC) casting were used in the present study. The chemical composition of the alloys is presented in Table I. Samples measuring 15 mm × 15 mm × 10 mm were cut from the center of the ingots.

Two types of homogenization heat treatment were applied.

One-step homogenization: This process was conducted using steps similar to traditional homogenization. The specimens were heated from room temperature to 550 °C at a 5 °C min⁻¹ heating rate; held for 2, 4, 6, 8, and 10 hours sequentially; and then water quenched to room temperature. A schematic of one-step homogenization is presented in Figure 1(a).

Two-step homogenization: The two-step homogenization route is illustrated in Figure 1(b). During the first

step of heat treatment, the samples were heated from ambient temperature to 175 °C, 250 °C, and 300 °C and held for 4, 8, 12, and 24 hours. The samples were then water quenched to room temperature. Subsequently, in the two-step homogenization, the samples were put directly into a furnace at 550 °C, held for 10 hours, and then water quenched.

For the visible distribution of dispersoids, the homogenized samples were polished and etched using 0.5 pct HF for 90 seconds. An Olympus GX53 optical microscope in dark-field mode was used to observe the distribution of dispersoids. The image analysis software Olycia M3 was used to characterize the area fraction of the CDZ. A HITACHI SU5000 scanning electron microscope equipped with a Nordlys Max electron backscatter diffraction detector (EBSD) was used to observe the recrystallized microstructure and substructure of the deformed samples at step sizes of 2.0 and 0.4 μ m, respectively. To distinguish between low-angle boundaries and high-angle boundaries, the former is indicated by white lines, whereas the latter is shown as black lines. Substructures with a misorientation of less than 5° appear with thinner white lines, and those greater than 5° but less than 10° are shown with thicker white lines. TEM foils were prepared using a twin-jet machine with a solution of 25 pct nitric acid in methanol at temperatures ranging from –20 °C to –30 °C. Operated at 200 kV, a transmission electron microscope (TEM, JEM-2100F) equipped with energy dispersive X-ray spectroscopy (EDS) was used to observe the morphology of the dispersoids. TEM bright-field images were recorded near the <110> zone axis and {200} planes under two-beam diffraction conditions. The segregation of the element map was measured using an electron probe microanalyzer (Shimadzu EPMA-1720) operated at 15 kV with beam current of 100 nA, a step size of 1.2 μ m, and a dwelling time of 70 ms per point.

Microhardness was measured using a Wilson VH1102 Vicker hardness tester with a load of 50 g and a dwelling time of 20 seconds. Ten measurements were taken, and the average was calculated. Homogenized samples from the center of the ingots were machined into cylindrical specimens measuring 10 mm in diameter and 15 mm in length for compression tests. The compression tests were conducted using a Gleeble 3800 thermomechanical simulation unit. Thermocouples were welded on the surface of the specimens, and graphic foils were placed at both ends. During compression tests, specimens were heated at a heating rate of 10 °C s⁻¹ and held for 3 min to ensure a uniform temperature. The specimens were compressed with strain rates of 0.1 s⁻¹ at 500 °C to a total true strain of 1.2.

III. RESULTS

A. Distribution and Morphology of the α -Al(Mn,Cr)Si Dispersoids After One-Step Homogenization

For 6xxx aluminum alloys containing Mn and Cr elements, α -Al(Mn,Cr)Si dispersoids precipitate during homogenization heat treatment.^[14,24] In the present

Table I. Chemical Composition of Alloys Used in the Present Study

	Mg	Si	Cu	Fe	Mn	Cr	Zr	Al
Alloy Composition (Wt Pct)	1.03	0.98	0.44	0.09	0.47	0.28	0.10	bal.

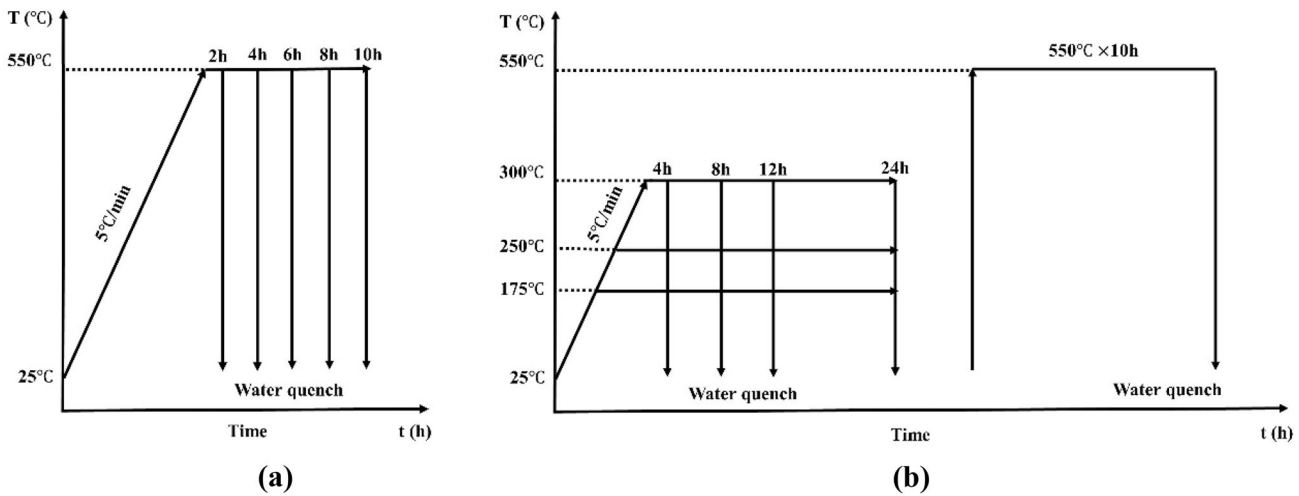


Fig. 1—Schematic diagrams of the (a) one-step homogenization heat treatment and (b) two-step homogenization heat treatment.

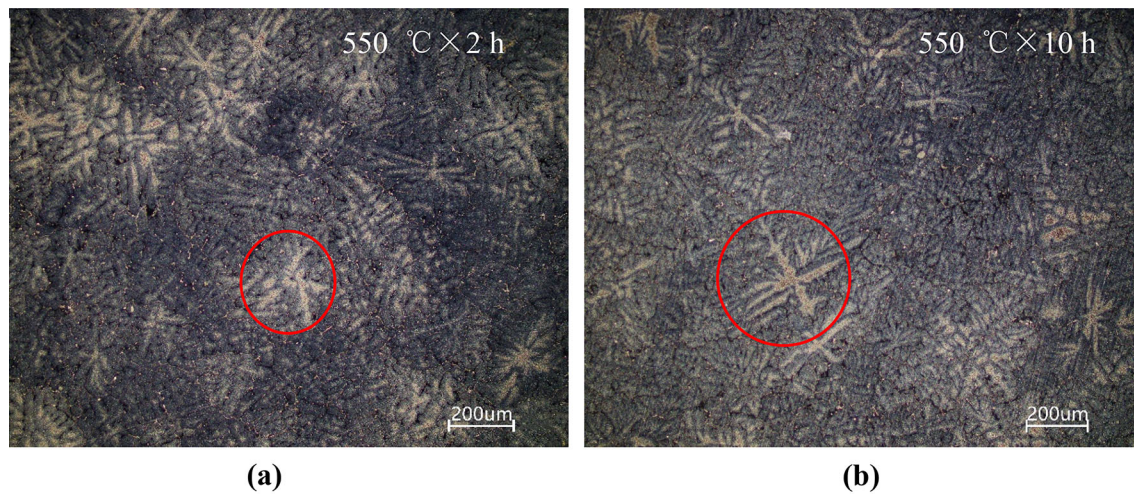
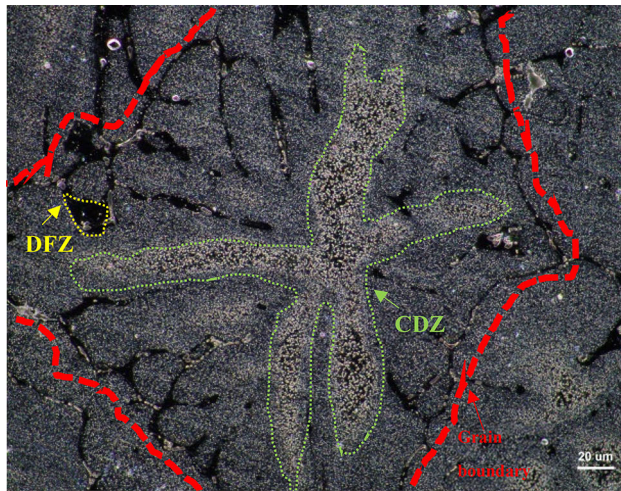


Fig. 2—Dark-field optical microscope images of one-step homogenized samples etched using 0.5 pct HF to indicate the nonuniform distribution of the dispersoids: (a) 550 °C × 2 hours and (b) 550 °C × 10 hours.

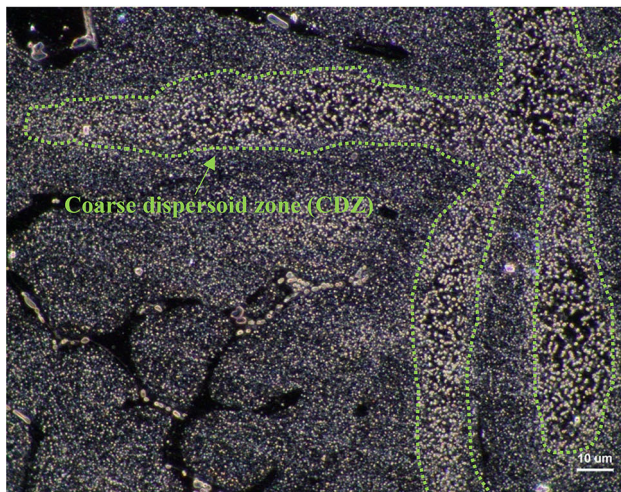
study, the samples were homogenized at 550 °C for different holding times. Owing to their small size, the α -Al(Mn,Cr)Si dispersoids were difficult to observe using an optical microscope. According to previous literature,^[6,7,12,17] after etching, the areas with a high density of dispersoids display a darker color. Therefore, in the present study, the samples were polished and etched to reveal the distribution of α -Al(Mn,Cr)Si dispersoids on a large scale by optical microscopy. Dark-field optical images are shown in Figures 2(a) and (b). Two colors were present in the etched samples, and some light-colored areas, marked in red circles in

Figures 2(a) and (b), were present at the center of dendritic arms. This result indicated that the distribution of dispersoids was not uniform. These uneven microstructures were present in both homogenized samples (2 hours × 550 °C and 10 hours × 550 °C), illustrating that the nonuniform distribution of dispersoids could not be completely removed by extending the holding time during homogenization.

The detailed morphology of the etched samples was observed at increased magnification (Figures 3(a) and (b)). α -Al(Mn,Cr)Si dispersoids were revealed by etching. Almost no dispersoids were present around grain



(a)



(b)

Fig. 3—Morphology of the coarse dispersoid zone of the samples homogenized at 550 °C for 10 hours: (a) and (b) dark-field optical microscope image.

boundaries. The grain boundaries of one grain are highlighted by a red dashed line as shown in Figure 3(a). Several black areas without dispersoids, also referred to as dispersoid-free zones (DFZs), were found within the interdendritic areas. These DFZs are well documented in previous literature.^[6,7,12,17] However, some dispersoids were sparsely distributed at the center of dendritic arms and are marked with a green dashed line. These dispersoids were also larger than the dispersoids in normal areas, hence the name coarse dispersoid zone or CDZ in the current study.

To confirm the validity of the aforementioned observation, nonetched samples were observed by SEM. The morphology of the dispersoids is shown in Figure 4. A nonuniform distribution of dispersoids was also observed. The dispersoids were evidently larger within the CDZ than in other areas. Samples under the same heat treatment conditions were also observed by TEM (Figure 5). Owing to the limited size of each observation

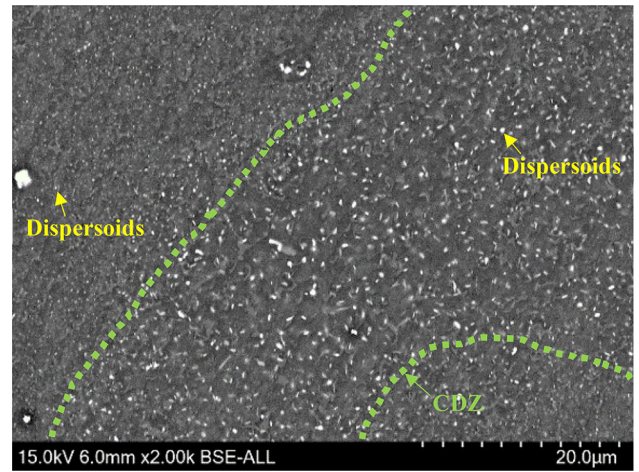


Fig. 4—SEM image of the distribution of dispersoids after homogenization at 550 °C for 10 hours.

view, nine figures were stitched together to present an overall view of the nonuniform distribution of dispersoids. The size of the dispersoids in the low-density areas was markedly larger. The distribution of dispersoids observed by TEM was consistent with that observed by optical microscopy and SEM. The chemical composition of the dispersoids was measured by EDS with TEM as shown in Figure 5(b), and Al, Mn, Cr, and Si were detected. Thus, on the basis of morphology^[25] and composition, the dispersoids were identified as α -Al(Mn,Cr)Si dispersoids.

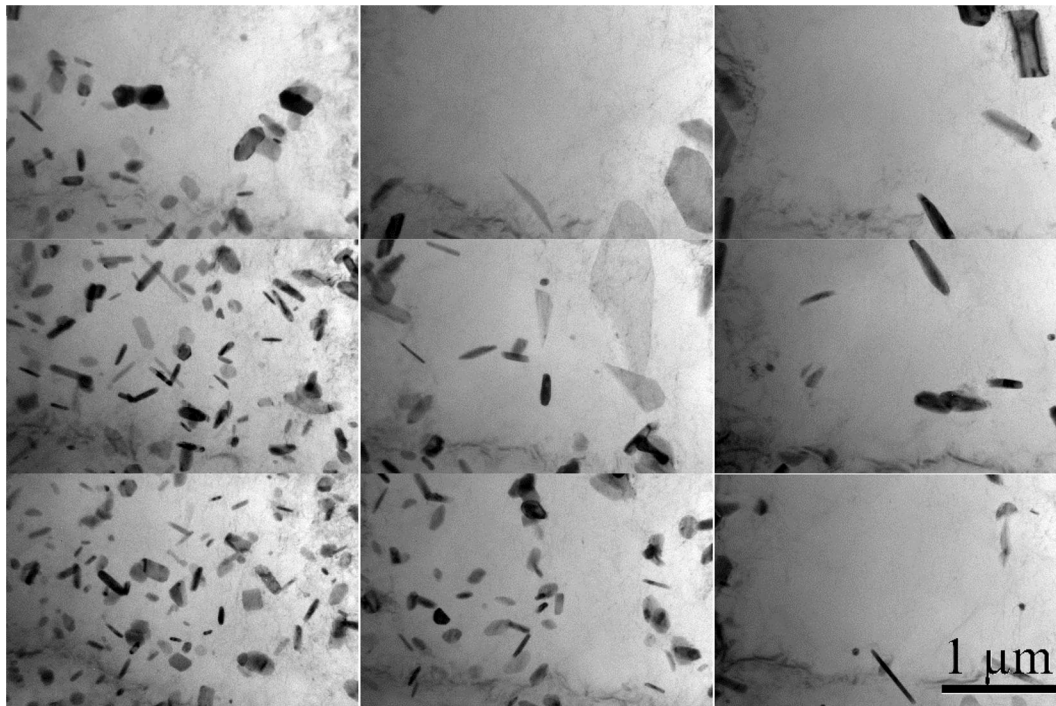
In summary, the existence of CDZ was confirmed based on the aforementioned observation. Moreover, the nonuniform distribution of the dispersoids was not removed by extending the holding time of the one-step homogenization process.

B. Effects of Two-Step Homogenization

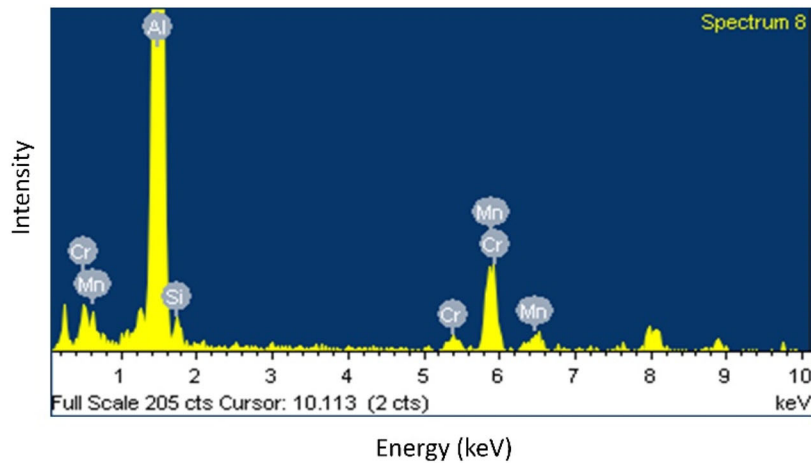
1. Distribution of dispersoids

To modify the nonuniform distribution of the dispersoids, two-step homogenization was conducted. The first step of the heat treatment was conducted at 175 °C, 250 °C, and 300 °C to precipitate metastable Mg_2Si or Q phases with different sizes. According to previous studies,^[11,14,15] metastable Mg_2Si or Q phases could act as nucleation sites for α -Al(Mn,Cr)Si dispersoids. The samples were then heat-treated at 550 °C for 10 hours as the second-step heat treatment, and the heating temperature and holding time were the same as those used in the one-step homogenization process.

Notably, the CDZ could hardly be observed after two-step homogenization, as shown in Figures 6(c) through (h). The percentage of CDZ area was quantified (Figure 7). The percentage of CDZ area of the samples heat-treated by single-step homogenization was approximately 7 pct. However, the percentage of CDZ area present in the samples heat-treated by two-step homogenization was only approximately 0.5 to 2.5 pct, regardless of the heating temperature and holding time during the first step of homogenization. This finding indicated



(a)



(b)

Fig. 5—After homogenization at 550 °C for 10 hours: (a) TEM images of the morphology and distribution of dispersoids and (b) chemical composition of α -Al(Mn,Cr)Si dispersoids.

that the uniformity of the dispersoids was markedly improved by two-step homogenization. As the temperature during the first step of heat treatment increased from 175 °C to 300 °C, the percentage of CDZ area continued to decrease. The minimum percentage was as low as 0.5 pct, and nearly all CDZs were removed. The holding time in the first step of heat treatment only slightly affected the CDZ amount. However, when the holding time was 4 hours, the percentage of CDZ area was slightly higher.

2. Size of the dispersoids

The details of the morphology of α -Al(Mn,Cr)Si dispersoids after one-step and two-step homogenization are shown in Figures 8(a) through (d). The images were taken from areas with a high density of dispersoids. According to previous literature,^[15] in 3xxx alloys, the size and type of metastable Mg_2Si influenced the size of dispersoids. In the present study, three different temperatures (175 °C, 250 °C, and 300 °C) were used in the first step of the heat treatment to precipitate various sizes and types of metastable Mg_2Si and Q phases.

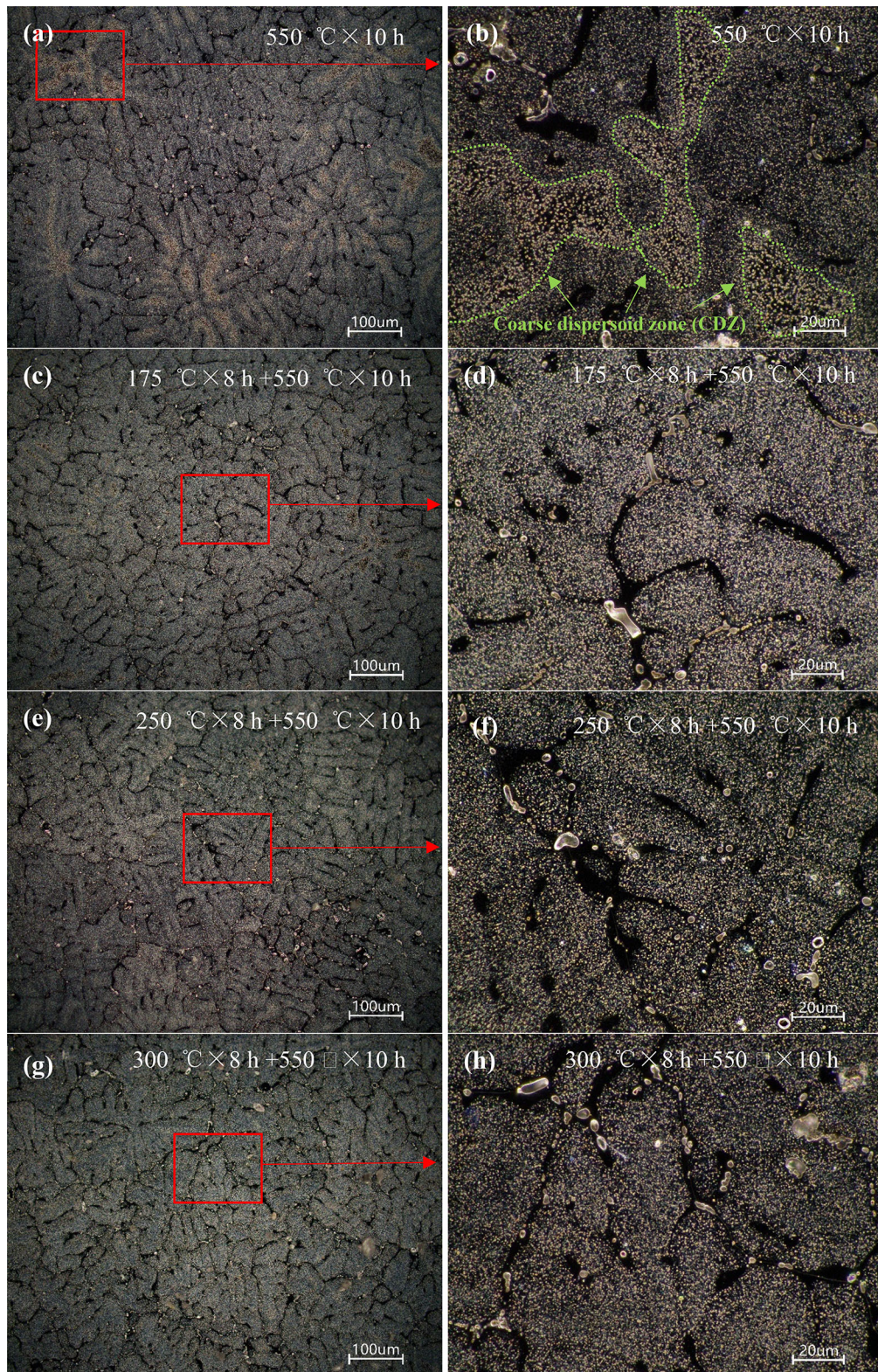


Fig. 6—Dark-field optical microscope images of the distribution of dispersoids: (a to b) 550 °C × 10 hours, (c to d) 175 °C × 8 hours + 550 °C × 10 hours, (e to f) 250 °C × 8 hours + 550 °C × 10 hours, (g to h) 300 °C × 8 hours + 550 °C × 10 hours.

However, a comparison of the sizes of dispersoids in the samples under different homogenization conditions indicated no apparent difference in size. This finding could be attributed to the high temperature and long

holding time of the second-step homogenization. The difference in size of the dispersoids probably still existed at the initial stages of dispersoid precipitation in 6xxx alloys, as mentioned in the literature.^[15] However, as the

α -Al(Mn,Cr)Si dispersoids fully coarsened, the difference in size was eliminated. The number densities were not comparable owing to the nonuniform distribution of the dispersoids in the samples subjected to one-step homogenization.

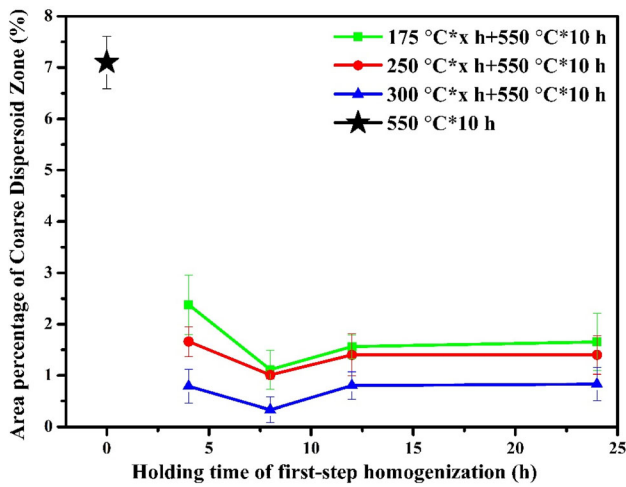


Fig. 7—Area percentage of the coarse dispersoid zone.

3. Microhardness

α -Al(Mn,Cr)Si dispersoids exerted a strengthening effect.^[25,26] Thus, microhardness test results could indirectly reveal the precipitation behaviors of the dispersoids. The microhardness test results are shown in Figure 9. First, the microhardness was tested within the CDZ of the samples subjected to one-step homogenization. The result was approximately 70, which was significantly lower than others, indicating a considerably smaller number of dispersoids. The hardness results of the CDZ showed a large error bar. This observation indicated that the distribution of dispersoids was not uniform within the CDZ. When the hardness of the sample subjected to one-step homogenization was measured regardless of the test area, the result obtained was approximately 90, which was 30 pct higher than the result for the CDZ. The samples subjected to two-step homogenization exhibited higher hardness owing to the smaller percentage of CDZ area. Owing to the variation in hardness measurement, the tendency of the hardness curves was imperfect. However, the samples subjected to a higher temperature during the first step of heat treatment tended to achieve higher hardness, which was inversely related to the percentage of CDZ area in Figure 7.

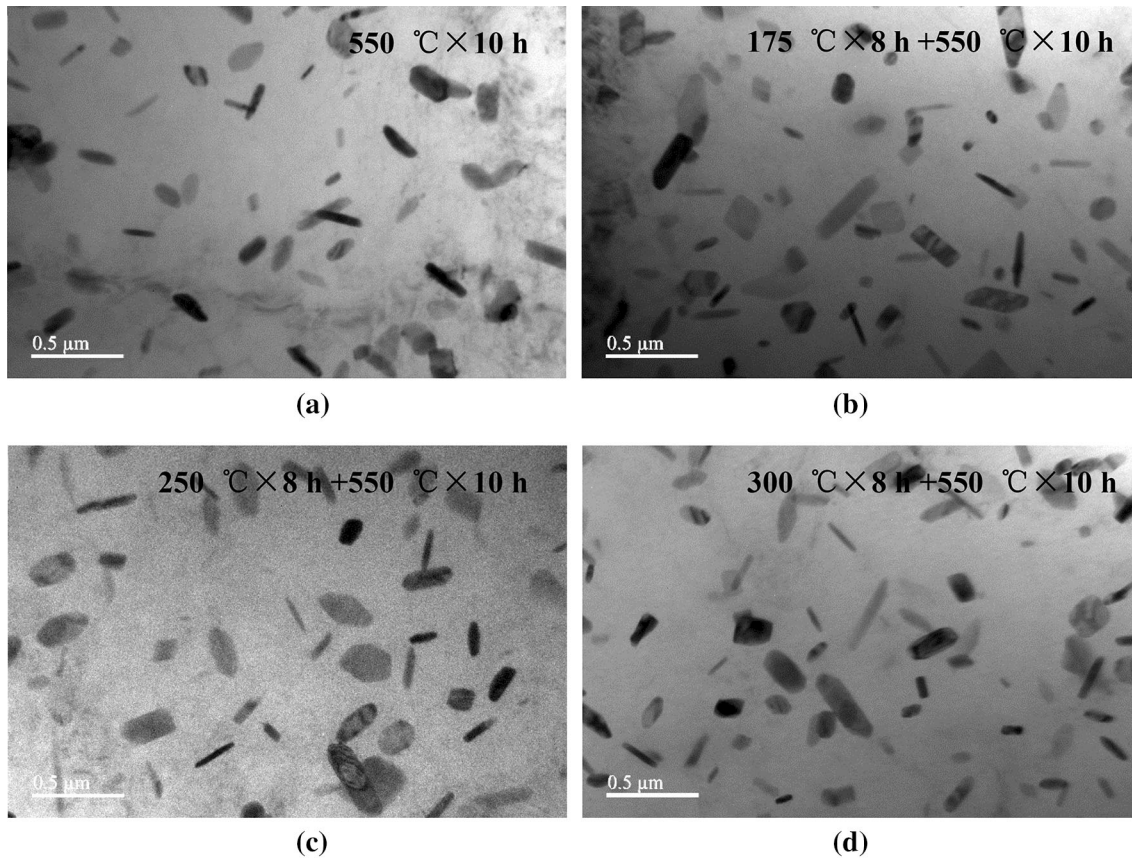


Fig. 8—TEM images of the morphology of the α -Al(Mn,Cr)Si dispersoids: (a) 550 °C × 10 hours, (b) 175 °C × 8 hours + 550 °C × 10 hours, (c) 250 °C × 8 hours + 550 °C × 10 hours, and (d) 300 °C × 8 hours + 550 °C × 10 hours.

4. Deformed microstructure

To evaluate the effect of the α -Al(Mn,Cr)Si dispersoid distribution on the hot deformation microstructure, cylindrical samples subjected to different homogenization heat treatments were compressed using a Gleeble machine at 500 °C at a strain rate of 0.1 s⁻¹ to 1.2 strain. The hot deformation microstructures are presented in dark-field optical images (Figure 10) and EBSD maps (Figure 11). In Figure 10(a), the elongated CDZ or DFZ perpendicular to the compression direction is present in the samples subjected to one-step homogenization. Thus, plastic deformation could not eliminate the nonuniform distribution of dispersoids. Moreover, the microstructures of samples subjected to two-step homogenization exhibited a more uniform distribution of α dispersoids apart from several elongated DFZs as shown in Figure 10(b).

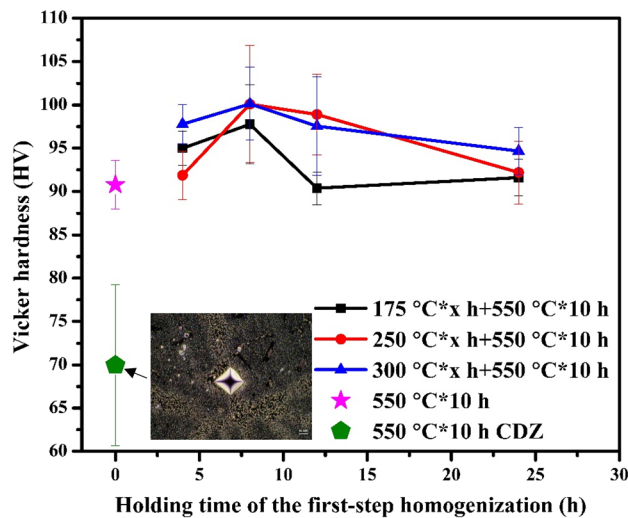


Fig. 9—Microhardness as a function of holding time in the first step of homogenization.

EBSD was employed to further examine the effect of the α -Al(Mn,Cr)Si dispersoid distribution on the dynamic softening mechanism of the alloy in this study. Typical EBSD inverse pole figure (IPF) maps of the deformed microstructure of the samples homogenized at 550 °C × 10 hours and 300 °C × 8 hours + 550 °C × 10 hours are shown in Figures 11(a) through (d), respectively. Maps were scanned perpendicular to the compression direction (CD), and followed the same IPF coloring as shown in Figure 11(e).

Low-magnification EBSD maps representing deformed and recrystallized microstructures are presented in Figures 11(a) and (c). The microstructures under both conditions contained elongated original grains and fragmented recrystallized grains primarily distributed along original grain boundaries. To further characterize the details of the deformation microstructure, EBSD tests at increased magnification were conducted in the center zone of Figures 11(a) and (c) and are marked by a white frame. The results are shown in Figures 11(b) and (d). Numerous subgrain boundaries were observed within the interiors of the original grains, indicating that the dynamic softening mechanism of the alloy in this study was a combination of dynamic recovery and recrystallization.

In the samples subjected to one-step homogenization, some recrystallized grains were distributed within the interior of the original grains and are marked by the black frame in Figure 11(b). Additionally, in the samples subjected to two-step homogenization, recrystallization within the grains was barely observed, as shown in Figure 11(d). This occurrence was strongly related to the amount of CDZs. Recrystallizations occurred in the CDZ because of the small number of dispersoids. For both the one-step and two-step homogenization samples, some recrystallized grains were distributed along the original grain boundaries, as shown in Figures 11(b) and (d). This occurrence was attributed to the DFZ near the original grain boundaries, which resulted in the lack of resistance to recrystallization.

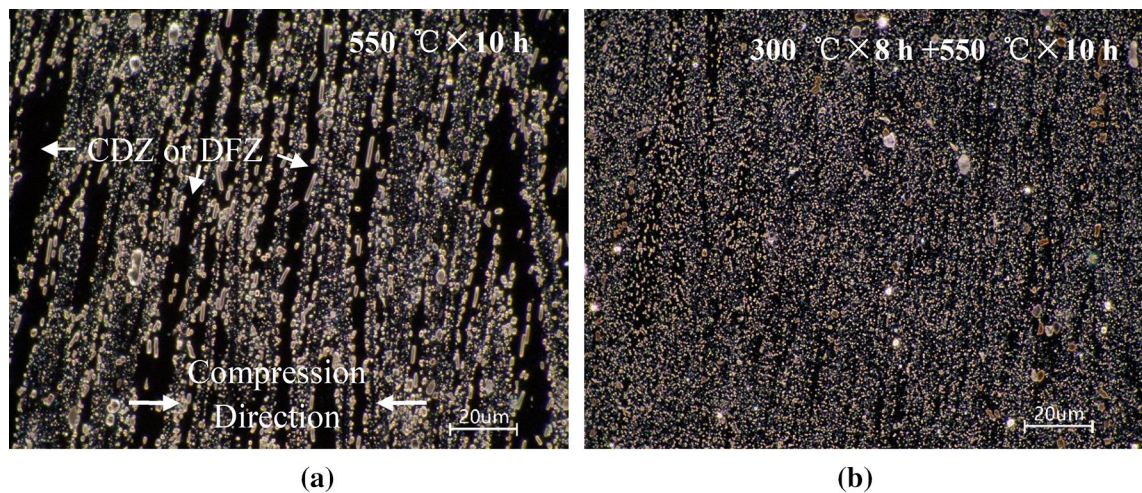


Fig. 10—Distribution of α -Al(Mn,Cr)Si dispersoids in the homogenized samples after hot deformation: (a) 550 °C × 10 hours, (b) 300 °C × 8 hours + 550 °C × 10 hours.

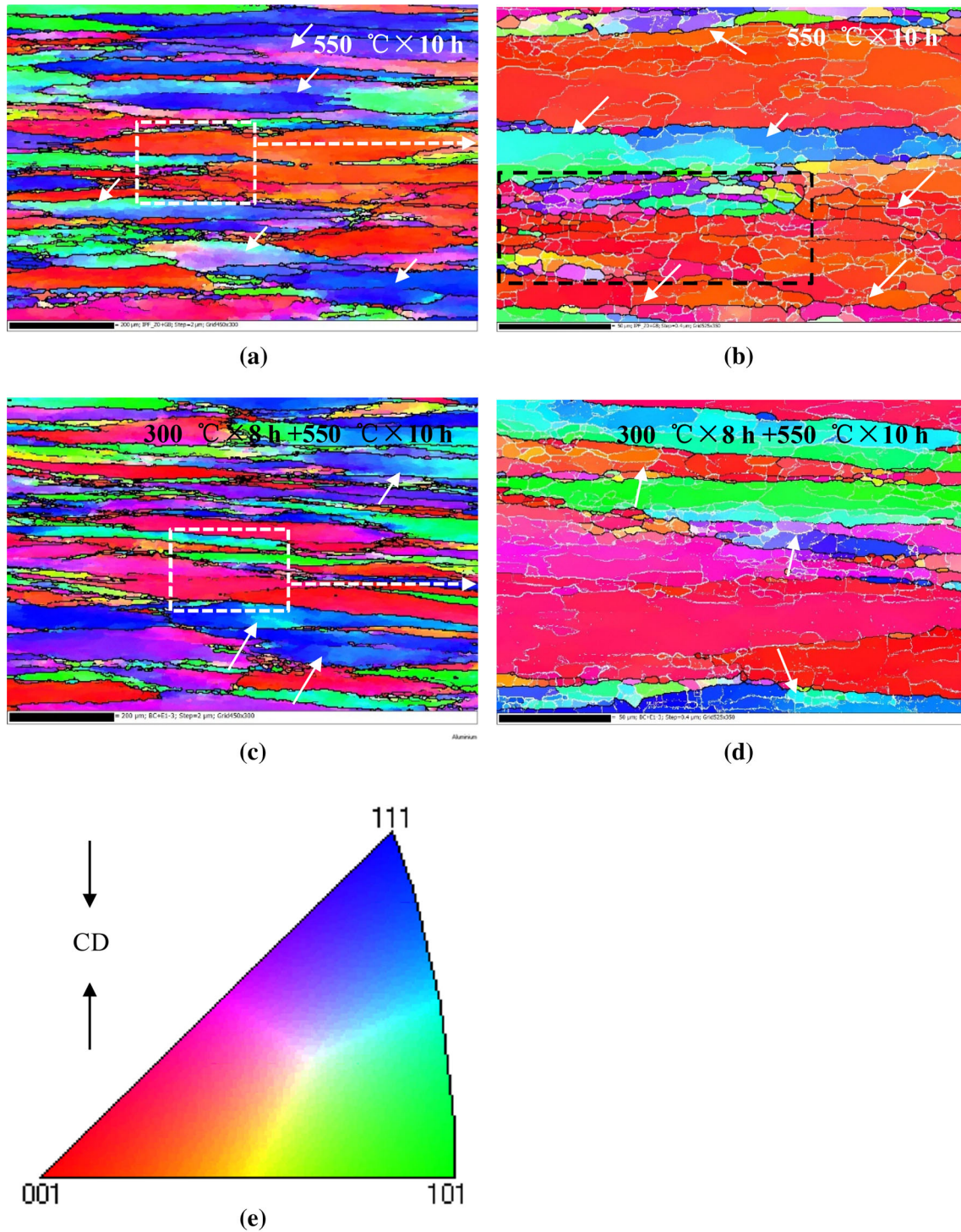


Fig. 11—Typical EBSD IPF maps of hot deformation samples subjected to homogenization: (a) 550 °C × 10 h, low magnification, (b) 550 °C × 10 h, high magnification, (c) 300 °C × 8 h + 550 °C × 10 h, high magnification, (d) 300 °C × 8 h + 550 °C × 10 h, high magnification, and (e) inverse pole figure coloring and CD.

Figure 11 shows IPF images, and the color difference of adjacent subgrains presents the misorientation between them.^[27] An evident misorientation between subgrains indicated the lack of limitation for migration of substructures in that area. In Figures 11(a) and (b), many regions presented distinct misorientation, as denoted by white arrows. Conversely, considerably

fewer regions were revealed by obvious misorientation in Figures 11(c) and (d). Moreover, the subgrain boundaries in Figure 11(d) are thinner than those in Figure 11(b). This difference also indicated that the misorientation in the sample subjected to two-step homogenization was lower than that subjected to one-step homogenization.

Combined with the results in Figure 10, the dynamic recrystallization and dynamic recovery of microstructures strongly depended on the distribution of dispersoids. The area fraction of the recrystallized region increased with the amount of CDZs and DFZs. The sample with uniformly distributed dispersoids presented fewer recrystallized regions and less substructural misorientation. Consequently, samples subjected to two-step homogenization showed increased recrystallization resistance during subsequent heating, improving the mechanical properties and corrosion resistance.

IV. DISCUSSION

A. As-cast microstructure analysis

To fully clarify the microstructure, the phases in the as-cast samples were observed at different scales. As shown in Figure 12(a), black Mg_2Si and bright $\text{Al}(\text{Mn}, \text{Fe}, \text{Cr})\text{Si}$ intermetallics were present along grain boundaries and in interdendritic areas, and sphere-shaped AlCuMgSi intermetallics were distributed inside grains. It is worth mentioning that all these phases contained Si and most of them were distributed along grain boundaries.

In terms of solute element distributions, EPMA tests of Si, Mg, Cu, Mn, Cr, and Fe were conducted. Quantitative elemental distribution maps of the as-cast samples corresponding with their backscattered electron images (Figure 12(a)) are presented in Figures 12(b) through (i).

The solute segregation trends of Si, Mg and Cu were similar: the content of solutes was lower at the center of grains and dendritic arms and gradually increased toward grain boundaries, as shown in Figures 12(b) (d), and (f). This observation is known as positive segregation, which is a common defect in aluminum alloys. Positive segregation was the result of solute redistribution at the solid–liquid interface during solidification and corresponded to the solute partition coefficient $k = C_S/C_L < 1$. Notably, k can properly characterize the tendency of solute element redistribution and the degree of solute segregation.^[28] The greater k deviates from 1, the stronger the tendency of positive or negative segregation for the solute.^[28] In the present study, the partition coefficient at the eutectic temperature was estimated according to the binary equilibrium phase diagram. The partition coefficient of Si, Mg, and Cu were $k_{\text{Si}} = 0.13$, $k_{\text{Mg}} = 0.43$, $k_{\text{Cu}} = 0.17$, respectively, which agreed with the positive segregation observed in the EPMA results. Si and Cu exhibited more serious segregation than Mg. If we enlarged the microsegregation areas (Figures 12(c) and (d)), the content of Si could often be found to be less than 0.1 pct at the center of dendritic arm, which is due to the limited solubility of Si at room temperature and formation of serious microsegregations. On the other hand, the lowest content of Mg at the center of dendritic arm could still reach about 0.5 pct, because of the high

Fig. 12—Backscattered electron images with corresponding elemental distribution maps of the as-cast samples, (a) backscattered electron images of the as-cast samples, (b) elemental distribution map of Si, (c) elemental distribution map of the Si segregation areas, (d) elemental distribution map of Mg, (e) elemental distribution map of the Mg segregation areas, (f) elemental distribution map of Cu, (g) elemental distribution map of Mn, (h) elemental distribution map of Cr, and (i) elemental distribution map of Fe.

solute limit and partition coefficient of Mg. It is worth mentioning that the positive segregations of Si, Mg, and Cu are similar to the distribution of the CDZ; the inherent reason will be discussed later.

In contrast, Mn and Cr tended to be abundant at the center of the grains and dendritic arm but poor along the grain boundaries and interdendritic areas, as shown in Figures 12(g) and (h). This result is the typical distribution of negative segregations ($k_{\text{Mn}} > 1$, $k_{\text{Cr}} > 1$), and agrees with the two-phase regions in binary Al–Mn and Al–Cr equilibrium phase diagrams.

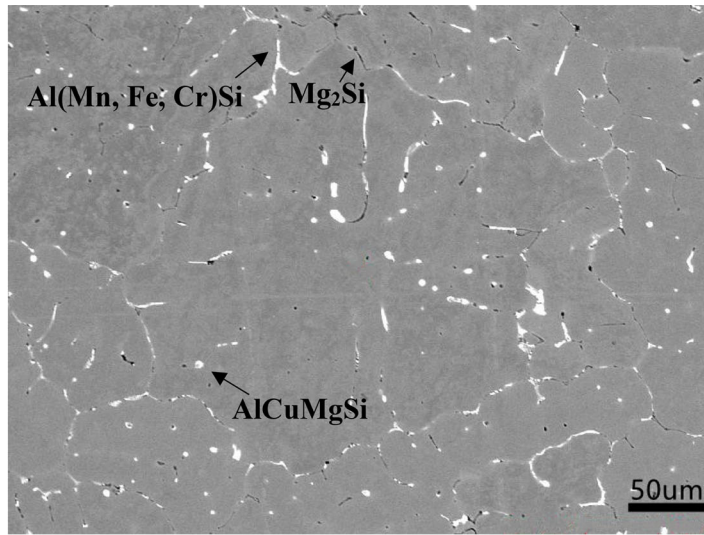
Fe was mainly present within the intermetallics, and very little Fe was present in the form solute atoms within grains (less than 0.06 wt pct) as shown in Figure 12 (i). Based on the Al–Fe phase diagram, the solubility of Fe in aluminum at room temperature could be neglected. As a result, no segregation of solute Fe was observed.

B. Analysis of the Microstructure After the First-Step Heat Treatment

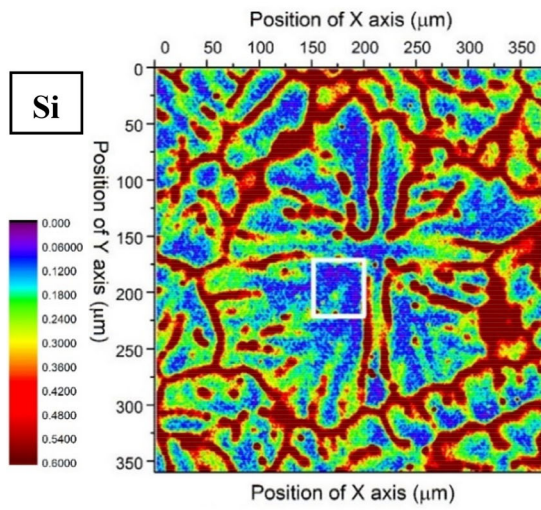
After heat treatment at 300 °C for 8 hours, the morphology of the intermetallic particles Mg_2Si , $\text{Al}(\text{Mn}, \text{Fe}, \text{Cr})\text{Si}$ and AlCuMgSi did not change much, as shown in Figure 13(a). Low-temperature heat treatment could not dissolve large intermetallic particles. However, according to the transmission electron microscopy observations (Figure 14), a large number of needle-like phases precipitated, and the size reached a few hundred nanometers because of over-aging.

Figures 13(b), (d), (f), (g), (h), and (i) show the distributions of solute elements after thermal holding at 300 °C for 8 hours. In general, the positive segregation of Si, Mg, and Cu could still be clearly observed, and isothermal holding did not thoroughly eliminate the microsegregation. However, compared to the as-cast sample, the percentage of segregation area of the 300 °C × 8 hours heat-treated samples decreased slightly; for example, the percentage of Si segregation areas ($\text{Si} \leq 0.1$ wt pct) dropped from 28.88 to 19.01 pct. Moreover, the segregation areas in the as-cast samples tended to be one large piece as shown in Figure 12(b). In the 300 °C × 8 hours heat-treated samples, the segregation areas were cut into many smaller pieces (Figure 13(b)).

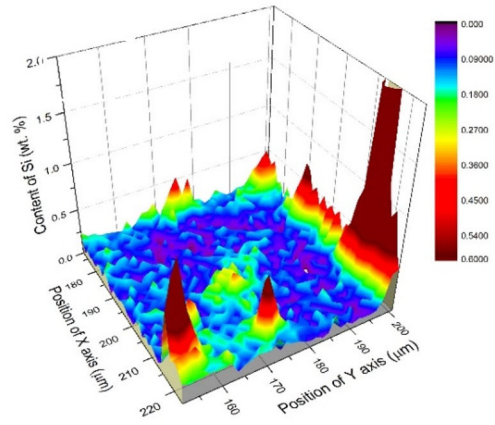
The distributions of Mn and Cr were not affected much due to heat treatment, and the segregation areas still existed along grain boundaries and interdendritic areas. This result can be attributed to the sluggish diffusion rate of Mn and Cr in aluminum at low temperature.^[29]



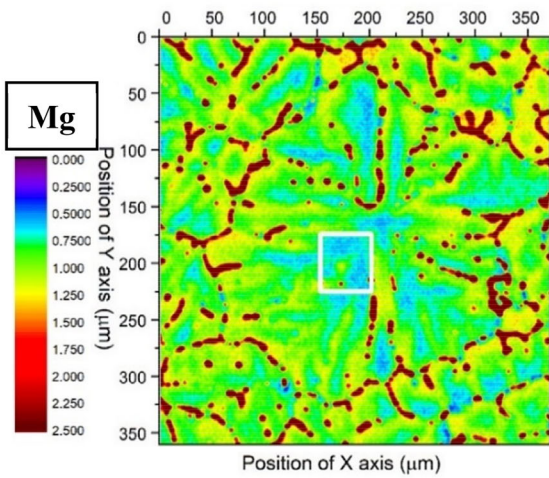
(a)



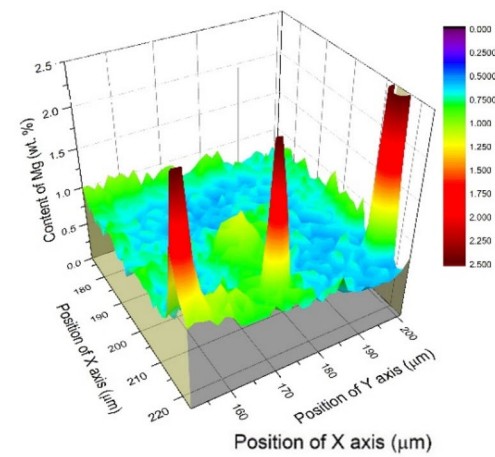
(b)



(c)



(d)



(e)

C. Possible Mechanism

1. Origin of CDZ formation

As shown in Figures 3(a) and 12(b), (d), and (f), the morphology of the CDZ was strongly consistent with the positive segregation in the as-cast microstructure. This result suggested that some Si, Mg, and Cu solute elements were responsible for the formation of CDZ during one-step homogenization. In contrast, Mn and Cr were abundant in the CDZ areas; thus, Mn and Cr were unlikely to be related to the formation of the CDZ, although Mn and Cr were essential for the precipitation of α -Al(Mn,Cr)Si dispersoids.

Regarding Si, according to the quantitative EPMA maps of the as-cast sample (Figures 12(b) and (c)), 28.8 pct of the area was Si segregation zones with less than 0.1 wt pct Si in solid solution. Moreover, Si was one of the essential elements for the nucleation and precipitation of α -Al(Mn,Cr)Si dispersoids. Therefore, Si segregation was the most likely origin of the CDZ.

In terms of Mg, because of the large solubility of Mg in aluminum, the lowest concentration of Mg could still reach approximately 0.5 pct, as shown in Figures 12(d)

Fig. 13—Backscattered electron images with their corresponding elemental distribution maps of samples heat-treated at 300 °C for 8 hours: (a) backscattered electron images of the heat-treated samples, (b) elemental distribution map of Si, (c) elemental distribution map of Si segregation areas, (d) elemental distribution map of Mg, (e) elemental distribution map of Mg segregation areas, (f) elemental distribution map of Cu, (g) elemental distribution map of Mn, (h) elemental distribution map of Cr, and (i) elemental distribution map of Fe.

and (e). Mg was not an essential element for α -Al(Mn,Cr)Si dispersoids, but affected the nucleation of α -Al(Mn,Cr)Si dispersoids. Mg could cause the formation of the CDZ by influencing nucleation, but due to the relatively sufficient supply in CDZ areas, the segregation of Mg may not be the most important reason for the CDZ.

In regard to Cu, our previous study^[11] showed that Cu had an influence on the size of α -Al(Mn,Cr)Si dispersoids, but an effect on dispersoid distribution was not observed.

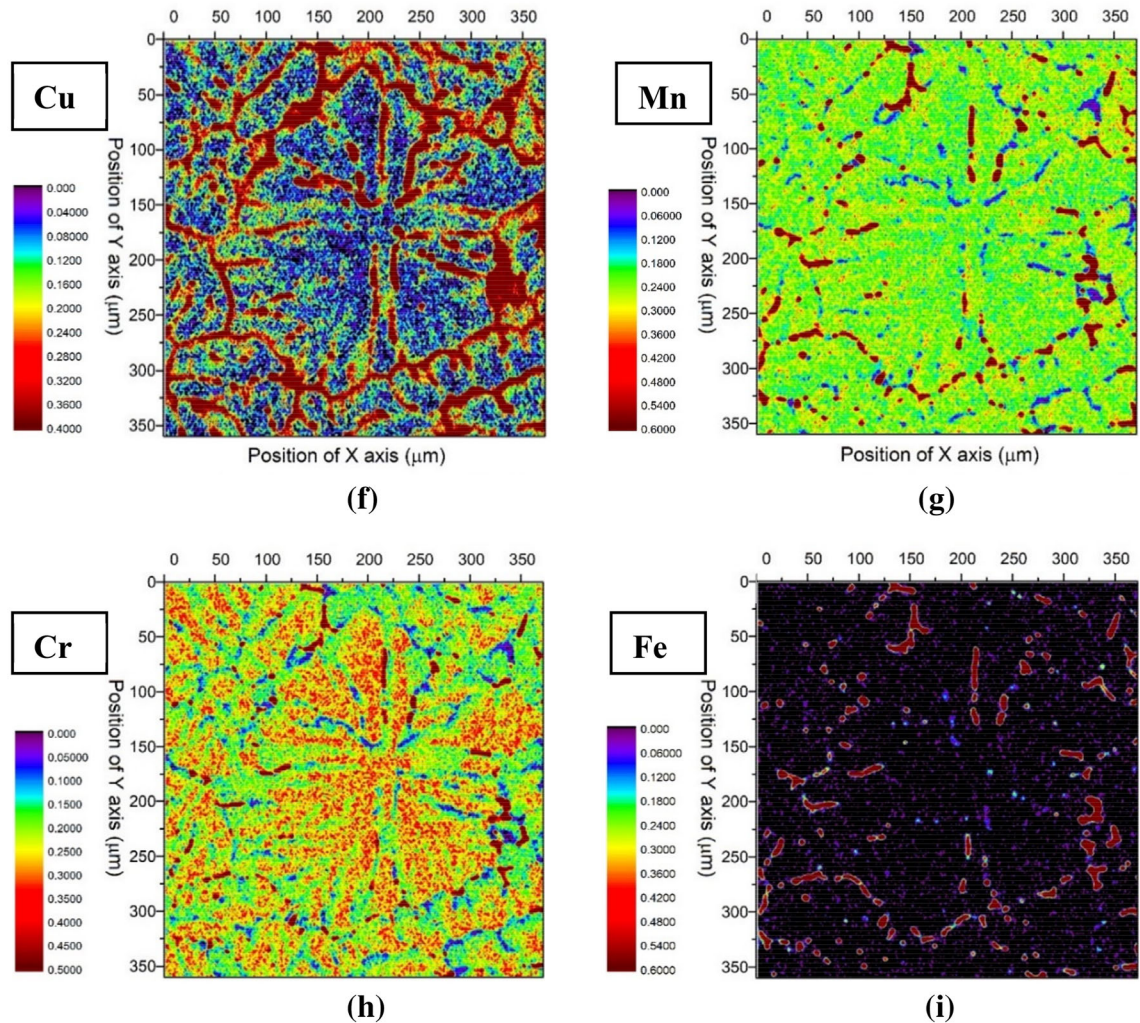
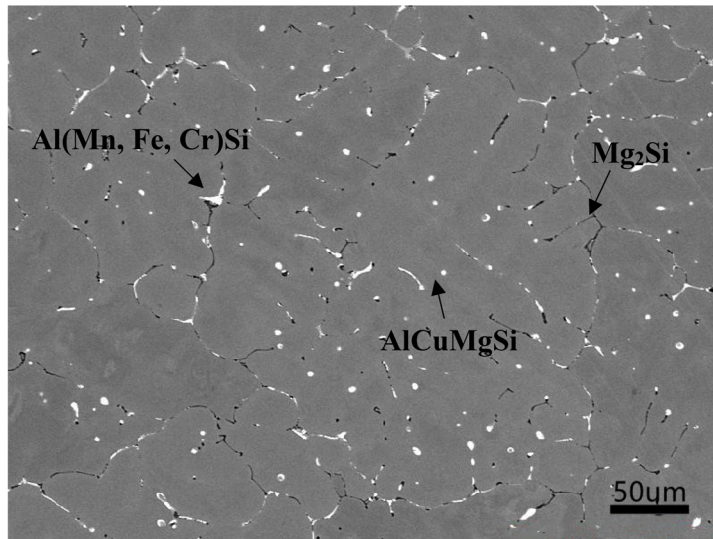
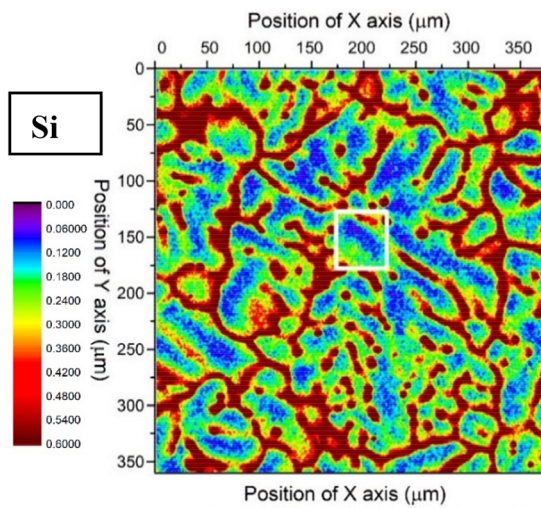


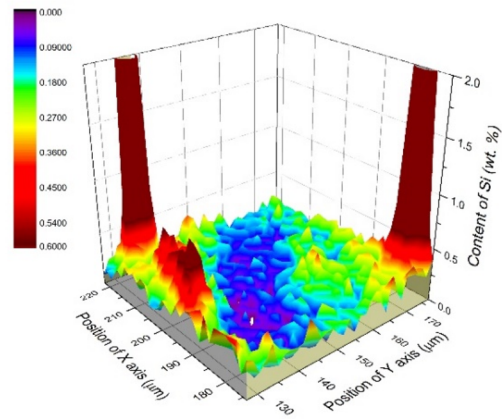
Fig. 12—continued.



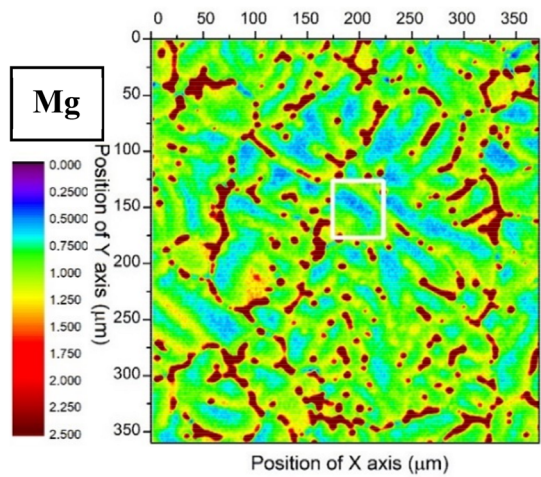
(a)



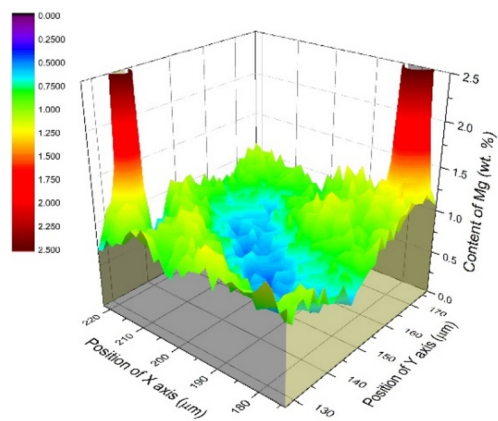
(b)



(c)



(d)



(e)

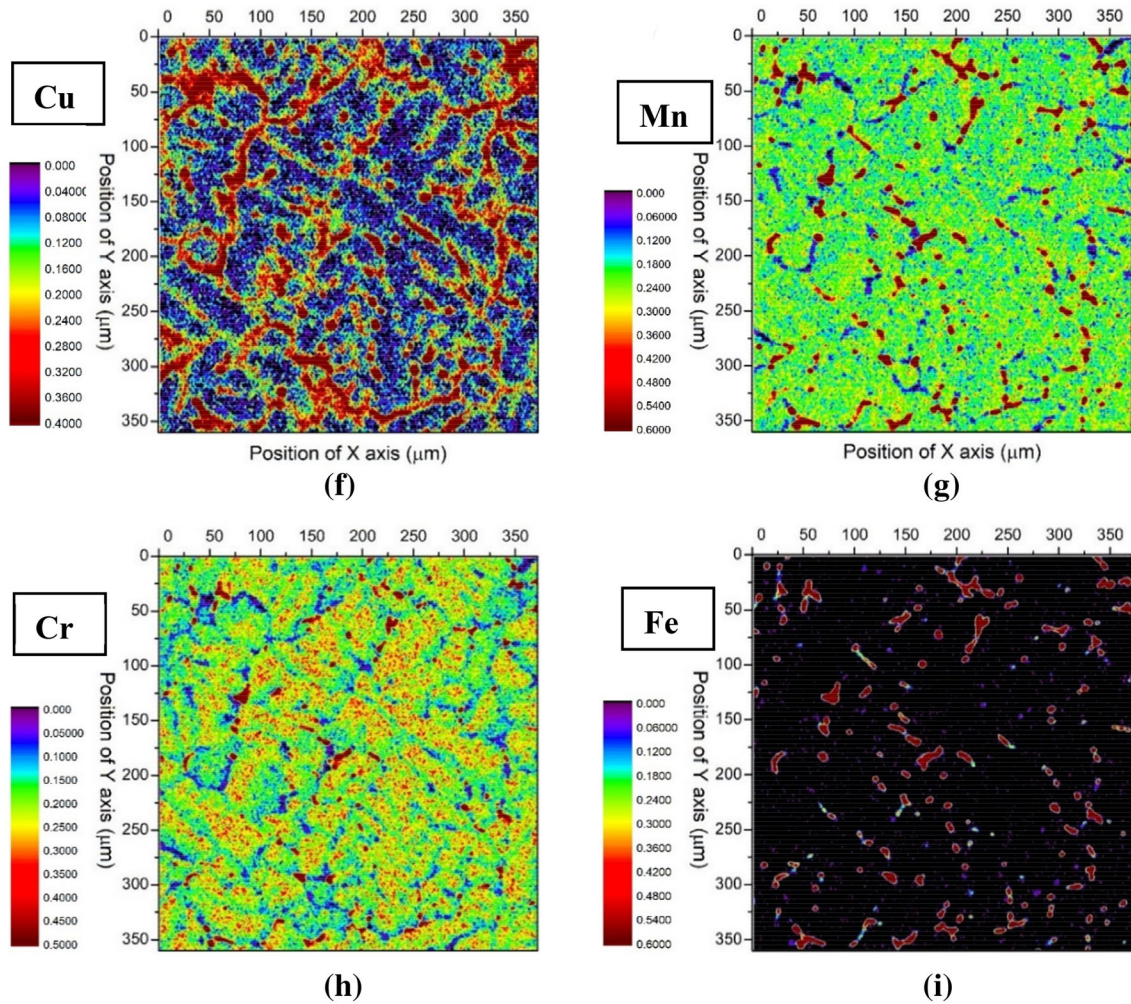


Fig. 13—continued.

2. Two-step homogenization

Evidently, two-step homogenization could significantly modify the distribution of α -Al(Mn,Cr)Si dispersoids. This observation could be attributed to the two aspects of transformations that occurred during the first isothermal holding step: diffusion and nucleation.

(a) Diffusion: As discussed above, the microsegregations were relieved slightly after the first-step isothermal heat treatment. Although the positive segregations were not completely removed, the diffusion process was still very important for Si, whose concentration was nearly zero in some of the most serious segregation areas. As the temperature increased, the diffusion coefficient of Si in Al increased dramatically.^[30,31] As the first-step isothermal temperature increased from 175 °C to 300 °C, the percentage of CDZ area decreased from approximately 2 to 1 pct, as shown in Figure 7. This result indicated that diffusion definitely had positive effects on the elimination of the CDZ. However, the most obvious change occurred when the sample conditions changed from 550 °C \times 8 hours to 175 °C \times 4 hours + 550 °C \times 8 hours, and the fractions of CDZ area decreased from 7 to 2.5 pct. Therefore, in the present study,

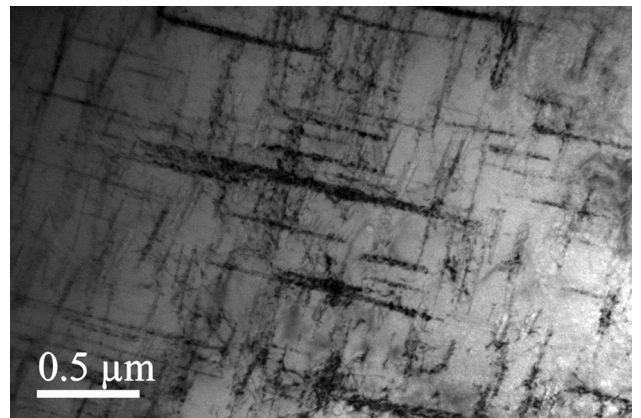


Fig. 14—TEM image of the samples heat-treated at 300 °C for 8 hours.

diffusion seemed not to be the most effective factor that affected the percentage of CDZ area.

(b) Nucleation: As the diffusion of solute elements continued during the first heat-treatment step, nanoscale metastable β -Mg₂Si and Q-AlMgSiCu phases

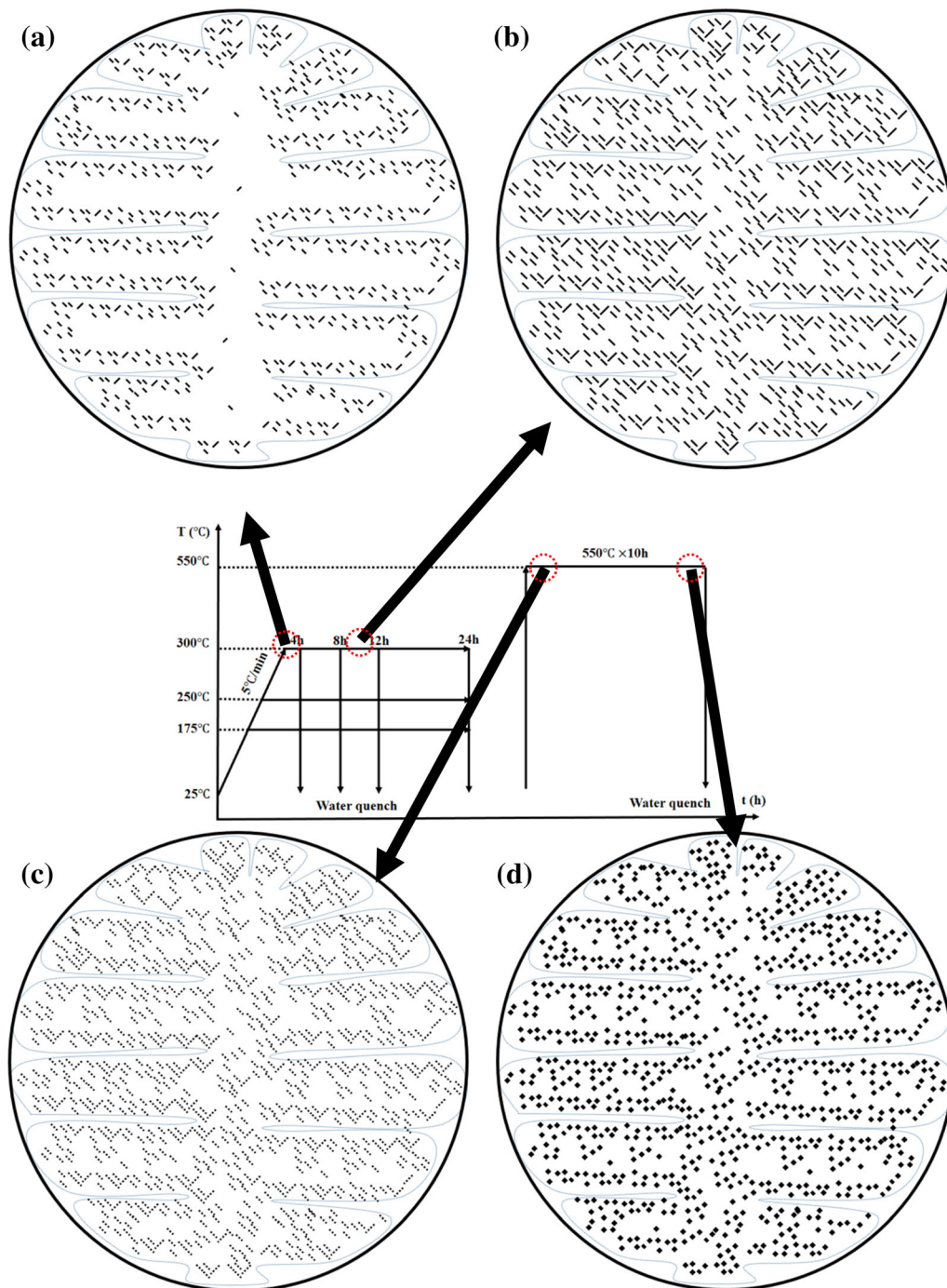


Fig. 15—Schematic of dispersoid formation during two-step homogenization: (a) precipitation of metastable Mg_2Si and Q phases, (b) uniform precipitation of metastable Mg_2Si and Q phases because of the long holding time, (c) nucleation of $\alpha-Al(Mn, Cr)Si$ dispersoids along the metastable Mg_2Si and Q phases, and (d) coarsened $\alpha-Al(Mn, Cr)Si$ dispersoids.

precipitated, as shown in Figure 14. The size and type of the precipitates depended on the aging temperature and holding time. According to previous studies,^[13–15] regardless of the size, all these metastable $\beta-Mg_2Si$ or Q- $AlMgSiCu$ phases could act as nucleation sites for $\alpha-Al(Mn, Cr)Si$ dispersoids. The precipitation temperature of $\alpha\alpha\alpha-Al(Mn, Cr)Si$ dispersoids started from approximately 340 °C,^[6] which was also in the

temperature range for dissolving $\beta-Mg_2Si$ and Q- $AlMgSiCu$. The phase transformation temperature overlap made heterogeneous nucleation possible. During the dissolution of the $\beta-Mg_2Si$ or Q- $AlMgSiCu$ phases, Si atom clusters were released, and then $\alpha-Al(Mn, Cr)Si$ dispersoids started to nucleate at the original locations of the dissolved $\beta-Mg_2Si$ or Q- $AlMgSiCu$ phases and took advantage of the Si atom clusters.^[15] Si was not

only the essential element for α -Al(Mn,Cr)Si dispersoid precipitation but also accelerated the precipitation rate.^[7,12] With the help of Si clusters provided by the dissolution of β -Mg₂Si and Q-AlMgSiCu, the precipitation of α -Al(Mn,Cr)Si dispersoids was dramatically promoted.^[12] Therefore, the uniform distribution of metastable β -Mg₂Si and Q-AlMgSiCu was extremely important for the uniform distribution of α -Al(Mn,Cr)Si dispersoids.

If traditional one-step homogenization was applied, the heating temperature would rapidly surpass the precipitation temperature range of metastable Mg₂Si or Q phases (150 °C to 350 °C). In the case of the present study, at a heating rate 5 °C/min, samples only spent 40 minutes precipitating metastable Mg₂Si and Q phases. In the solute depleted zone, the precipitation of nucleation sites for α -Al(Mn,Cr)Si dispersoids would not be sufficient, due to the lack of driving force. For example, in the serious Si segregation zone, the precipitation of metastable Mg₂Si and Q phases would be extremely difficult. Thus, at the center of the grains and dendritic arms, inadequate metastable Mg₂Si and Q phases precipitated. As a result, when the heating temperature reached the precipitation temperature of α -Al(Mn,Cr)Si dispersoids, α -Al(Mn,Cr)Si dispersoids had to precipitate without nucleation sites, which led to the formation of a CDZ.

Notably, if two-step homogenization was applied, the first step of heat treatment would provide Mg and Si sufficient time to precipitate. The isothermal holding during the first step of the heat treatment was especially important for precipitation in the severe segregation zones, where the driving force of precipitation was weak. Moreover, the diffusion of solute elements also helped to obtain a more uniform distribution of β -Mg₂Si and Q-AlMgSiCu. A more uniform precipitation of nucleation sites was expected to cause an improvement in the distribution of α -Al(Mn,Cr)Si dispersoids. Consequently, the amount of CDZ markedly decreased relative to that under one-step homogenization conditions. A schematic is presented in Figure 15 to demonstrate the nucleation and precipitation process of α -Al(Mn,Cr)Si dispersoids during two-step homogenization.

After homogenization at 550 °C, the size of the α -Al(Mn,Cr)Si dispersoids was a few hundred nanometers, as shown in Figure 8. Because of the low diffusion rate of Mn and Cr,^[29] α -Al(Mn,Cr)Si dispersoids were unlikely to further coarsen during subsequent hot processing. α -Al(Mn,Cr)Si dispersoids could effectively slow the movements of dislocations and subgrain boundaries. This observation was the reason why samples subjected to two-step homogenization showed increased recrystallization resistance. On the other hand, one-step homogenization samples may suffer from abnormal coarse grains in the CDZ areas, which led to a nonuniform mechanical properties and poor corrosion resistance.

V. CONCLUSIONS

1. The CDZ was distributed at the center of grains or dendritic arms. In accordance with the characterization of the dispersoids by optical microscopy, SEM, and TEM, the number density of the dispersoids was lower, and the size of the dispersoids was larger within the CDZ. During one-step homogenization at 550 °C, the CDZ could not be eliminated by extending the holding time from 2 to 10 hours.
2. Compared with one-step homogenization, two-step homogenization led to a considerable decrease in the percentage of CDZ area from approximately 7 pct to less than 2.5 pct. As the first-step heating temperature increased from 175 °C to 300 °C, the amount of CDZ further decreased from 2.5 to approximately 1 pct.
3. Plastic deformation could not eliminate the nonuniform distribution of α -Al(Mn,Cr)Si dispersoids caused by the CDZs and DFZs. Recrystallized grains in the deformed sample by one-step homogenization were distributed not only along the original grain boundaries but also within the interior of the original grains. However, the recrystallized grains in the deformed sample subjected to two-step homogenization were distributed only along the original grain boundaries. This observation indicated that two-step homogenization significantly decreased the areas where dynamic recrystallization tended to occur, because of the decrease in the percentage of CDZ area.
4. Microsegregation of Mg and Si caused by casting led to the uneven distribution of metastable Mg₂Si and Q phases, which were the nucleation sites of α -Al(Mn,Cr)Si dispersoids. Consequently, the α -Al(Mn,Cr)Si dispersoids precipitated in a nonuniform manner, and a CDZ was formed.
5. Two-step homogenization could significantly modify the distribution of α -Al(Mn,Cr)Si dispersoids. This observation could be attributed to the diffusion of Si and Mg solute elements and, more importantly, the sufficient precipitation of Mg₂Si and Q phases during the first step of isothermal holding. Mechanisms of dispersoid formation during two-step homogenization were proposed.

ACKNOWLEDGMENTS

The authors acknowledge the financial support provided by Shandong Weiqiao Pioneering Group Co., Ltd., National Natural Science Foundation of China (Grant No. U1864209) and China Postdoctoral Foundation Grant (Grant No. 2018M642309).

REFERENCES

1. W.H. Van Geertruyden, H.M. Browne, W.Z. Misiolek, and P.T. Wang: *Metallurgical and Materials Transactions A*, 2005, vol. 36, pp. 1049–56.
2. A.R. Eivani, J. Zhou, and J. Duszczyk: *Philosophical Magazine*, 2016, vol. 96, pp. 1188–96.
3. Y. Xu, H. Nagaumi, Y. Han, G. Zhang, and T. Zhai: *Metallurgical and Materials Transactions A*, 2017, vol. 48, pp. 1355–65.
4. K. Huang, K. Zhang, K. Marthinsen, and R.E. Logé: *Acta Materialia*, 2017, vol. 141, pp. 360–73.
5. S. Tangen, K. Sjølstad, T. Furu, and E. Nes: *Metallurgical and Materials Transactions A*, 2010, vol. 41, pp. 2970–83.
6. K. Liu and X.G. Chen: *Materials & Design*, 2015, vol. 84, pp. 340–50.
7. Y.J. Li and L. Arnberg: *Acta Materialia*, 2003, vol. 51, pp. 3415–28.
8. K. Liu, H. Ma, and X.G. Chen: *Journal of Alloys and Compounds*, 2017, vol. 694, pp. 354–65.
9. Z. Li, Z. Zhang, and X.G. Chen: *Materials Science and Engineering: A*, 2018, vol. 729, pp. 196–207.
10. A.M.F. Muggerud, E.A. Mørtzell, Y. Li, and R. Holmestad: *Materials Science and Engineering: A*, 2013, vol. 567, pp. 21–28.
11. Z. Li, Z. Zhang, and X.-G. Chen: *Metals*, 2018, vol. 8, p. 155.
12. Z. Li, Z. Zhang, and X.G. Chen: *Materials Science and Engineering: A*, 2017, vol. 708, pp. 383–94.
13. H. Hirasawa: *Scripta Metallurgica*, 1975, vol. 9, pp. 955–58.
14. L. Lodgaard and N. Ryum: *Materials Science and Engineering: A*, 2000, vol. 283, pp. 144–52.
15. Z. Li, Z. Zhang, and X.G. Chen: *Metallurgical and Materials Transactions A*, 2018, vol. 49, pp. 5799–814.
16. C.L. Liu, Q. Du, N.C. Parson, and W.J. Poole: *Scripta Materialia*, 2018, vol. 152, pp. 59–63.
17. Q. Du, W.J. Poole, M.A. Wells, and N.C. Parson: *Acta Materialia*, 2013, vol. 61, pp. 4961–73.
18. Y. Birol: *Journal of Materials Processing Technology*, 2004, vol. 148, pp. 250–58.
19. N.C.W. Kuijpers, J. Tirel, D.N. Hanlon, and S. van der Zwaag: *Materials Characterization*, 2002, vol. 48, pp. 379–92.
20. S. Kumar, P.S. Grant, and K.A.Q. O'Reilly: *Metallurgical and Materials Transactions A*, 2016, vol. 47, pp. 3000–14.
21. N. Bayat, T. Carlberg, and M. Cieslar: *Journal of Physics and Chemistry of Solids*, 2019, vol. 130, pp. 165–71.
22. N. Bayat, T. Carlberg, and M. Cieslar: *Journal of Alloys and Compounds*, 2017, vol. 725, pp. 504–09.
23. H. Tanihata, T. Sugawara, K. Matsuda, and S. Ikeno: *Journal of Materials Science*, 1999, vol. 34, pp. 1205–10.
24. M.S. Remøe, I. Westermann, and K. Marthinsen: *Metals*, 2018, vol. 9, p. 26.
25. Y.J. Li, A.M.F. Muggerud, A. Olsen, and T. Furu: *Acta Materialia*, 2012, vol. 60, pp. 1004–14.
26. F. Qian, S. Jin, G. Sha, and Y. Li: *Acta Materialia*, 2018, vol. 157, pp. 114–25.
27. Q. Yang, Z. Deng, Z. Zhang, Q. Liu, Z. Jia, and G. Huang: *Materials Science and Engineering: A*, 2016, vol. 662, pp. 204–13.
28. R. Smith: *Metallurgical and Materials Transactions B*, 2018, vol. 49, pp. 3258–79.
29. K.E. Knipling, D.C. Dunand, and D.N. Seidman: *Zeitschrift für Metallkunde*, 2006, vol. 97, pp. 246–65.
30. M. Patrick Dugan, T. Tsakalakos: *Superlattices and Microstructures*, 1988, vol. 4, pp. 565–570.
31. S.-I. Fujikawa, K.-I. Hirano, and Y. Fukushima: *Metallurgical Transactions A*, 1978, vol. 9, pp. 1811–15.

Publisher's Note Springer Nature remains neutral with regard to jurisdictional claims in published maps and institutional affiliations.